STRUCTURE DESIGN OF POLOIDAL HORSESHOE LIMITER FOR PULSE OPERATION HEAT LOAD IN JA DEMO

W. Chen

National Institutes for Quantum Science and Technology Rokkasho/Aomori, Japan Email: chen.weixi@qst.go.jp

S. Sugiyama

National Institutes for Quantum Science and Technology Rokkasho/Aomori, Japan

N. Asakura

National Institutes for Quantum Science and Technology Naka, Japan

Y. Someya

National Institutes for Quantum Science and Technology Rokkasho, Japan

S. Kakudate

National Institutes for Quantum Science and Technology Naka, Japan

N. Umeda

National Institutes for Quantum Science and Technology Naka, Japan

H. Utoh

National Institutes for Quantum Science and Technology Rokkasho/Aomori, Japan

Y. Sakamoto

National Institutes for Quantum Science and Technology Rokkasho/Aomori, Japan

Abstract

In fusion reactor JA DEMO, a poloidal horseshoe limiter has been developed to protect the breeding blanket (BB) from excessive heat loads during plasma operation. The limiter protrudes from the first wall (FW) toward the plasma, shielding the BB from charged particle heat flux deposited along magnetic field lines. Key design features include continuous poloidal coverage (excluding the divertor), toroidal discretization, a curved surface in the toroidal direction, tungsten monoblock as plasma-facing units, reduced activation ferritic/martensitic (F82H) steel pipes as heat sinks, and 15.5 MPa pressurized water as coolant. The limiter is subjected to both surface heat load and volumetric nuclear heating. Among the components of the surface heat load, the charged particle heat load is highly localized and sensitive to changes in magnetic equilibrium. Using magnetic field line tracing via the APPLE code, the heat load was evaluated at key time points throughout anticipated pulsed plasma operation scenario. Peak heat fluxes of 2.8 MW/m² during the ramp-up phase and 1.9 MW/m² during the flat-top phase were observed. To assess the applicability of plasma-facing unit (PFU) designs, two configurations with different interlayer materials, copper and titanium, were analyzed using time-transient coupled thermal-structural simulations under ramp-up and flat-top heat load conditions. While copper provided high thermal conductivity, it resulted in elevated von Mises stress and plastic deformation due to its high thermal expansion, increasing the risk of cracking. In contrast, titanium reduced stress by 52%, maintained elastic deformation, and shifted stress concentration to the outer surface of the F82H pipe, thereby enhancing structural integrity. These findings demonstrate that titanium interlayers significantly improve the durability and reliability of PFUs under high-heat-flux conditions, making them a promising candidate for fusion reactor applications.

1. INTRODUCTION

The limiter is one of the plasma facing components in tokamak nuclear fusion reactor, which is designed for protecting the breeding blanket (BB) from excess heat load [1-5]. The concept of the limiter is protruding its surface from the first wall (FW) towards the plasma to shade the BB from the charged particle heat load, which

deposited on the FW alone side the magnetic field lines. The poloidal horseshoe limiter in JA DEMO has been proposed and developed [6-8], whose design characteristics are listed as follows.

- (a). Continue in poloidal direction except the divertor area.
- (b). Discretise in toroidal direction.
- (c). Curve surface in toroidal direction.
- (d). Apply tungsten mono-block as plasma facing unit.
- (e). Utilize reduced activation ferritic/martensite (F82H) pipes as heat sink.
- (f). Adopt 15.5 MPa pressurized water as coolant.

The first and most critical load for limiter design is the heat load. For plasma facing component, including the limiter, the heat load consists of two sources: surface heat load from the plasma power deposition and nuclear heating due to neutron irradiation. Nuclear heating is volumetric and can be simulated through nuclear analysis. The surface heat load includes the charged particle heat load, radiation heat load, charged exchange, ripple loss. The charged particle heat load refers to the power transferred from the core plasma to the FW via the scrape-off layer (SOL). The components except for the charged particle heat load are conservatively estimated to contribute a total heat flux of 0.5 MW/m² during flat-top phase [9]. Charged particle heat load tends to be highly localized, as the power is transferred by charged particles, and the charged particles cling to the magnetic field lines. During normal plasma operation, changes in magnetic equilibrium led to variations in magnetic field lines, which in turn cause fluctuations in in the heat flux distribution.

The charged particle heat load has been evaluated using APPLE code based on magnetic field lines tracing[9], and the concept of the limiter has been studied in several specific plasma phase in previous studies [8]. However, the adaptability of the plasma-facing unit (PFU) for the limiter throughout the plasma operation remains an open question, as transient heat load may create harsher conditions that accelerate thermal fatigue. In this study, the heat load on the limiter during anticipated pulsed plasma operation is evaluated, and two candidates PFU designs are assessed for their applicability based on thermal stress induced by heat load. To analyze the time-dependent heat load on the limiter, magnetic equilibriums at several time points during the operation were selected, and the corresponding charged particle heat loads were evaluated. Based on these evaluation, two types of transient high heat flux scenarios were simulated as input conditions for PFU. Thermal stresses on the proposed PFU designs were simulated and analyzed using finite element method (FEM) software. Design strategies to mitigate the thermal stress are also discussed.

2. MATERIAL AND METHOD

2.1. Pulsed plasma operation scenario in JA DEMO

Referring to the pulsed plasma operation scenario studied in previous study [10], the plasma current (I_p) at flattop phase reaches 12.3 MA. The change rates of I_p during ramp-up and ramp-down phase are 0.15 MA/s and -0.075 MA/s, respectively. The net plasma loss power across the separatrix (P_{sep}) is calculated using TOPICS code [11], based on the heat transport and power exhaust. The time evolution of I_p and P_{sep} is illustrated in Fig. 1(a).

These plasma parameters are used to generate magnetic equilibrium using TOSCA code [12]. Figures 1(b) and 1(c) show the time evolution of the plasma shape. The ramp-up phase begins with the plasma touching the inboard limiter. A transition from limiter configuration plasma to divertor configuration plasma occurs when I_p =4 MA, corresponding to 27 seconds after the start of operation. Heating begins at 66 seconds, followed by an L-H transition at 70 seconds. The plasma reaches flat-top phase at 88 seconds, with a plasma current of 12.3 MA. Heating continues to achieve full-power operation. After maintaining the flat-top plasma for two hours, the plasma ramp-down phase begins. The plasma is guided to touch the outboard limiter for a controlled termination. The magnetic equilibriums at distinctive time points are used to evaluate the charged particle heat load throughout the operation.

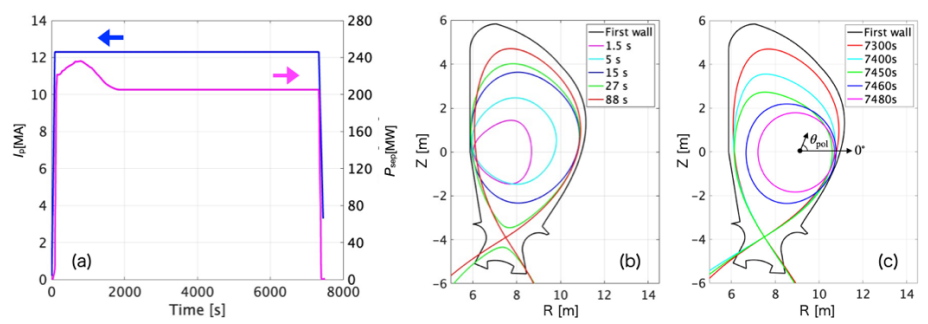


FIG. 1 Pulsed plasma operation scenario. The time evolution of (a) plasma current and $P_{\text{sep.}}$ (a) plasma shape during rampup and (b) plasma shape during ramp-down.

In evaluating the charged particle heat load, a decay length (λ) model for the SOL plasma is employed as the key plasma parameter. The heat flux is calculated by multiplying the heat flux that parallel to the magnetic field line (q_{ij}) by the incident angles between the magnetic field line and the FW. For the limiter configuration plasma, λ is estimated using approximation equation derived from experimental results across several tokamak devices [13-14].

$$\lambda = 0.63 \times \boldsymbol{B}_{\text{pol,MP}}^{-1.19}$$

Here, $B_{\text{pol},MP}$ represents the poloidal magnetic field at the outboard midplane, obtained from the magnetic equilibrium. The value of λ with plasma current during the ramp-up phase is shown in Fig. 2. After the L-H transition, the P_{sep} is assumed to be equally distributed by near SOL and far SOL, each contributing half of P_{sep} [15]. For the decay length, λ is assumed to be 1 mm for near SOL [16-17], and 50 mm for the far SOL [18].

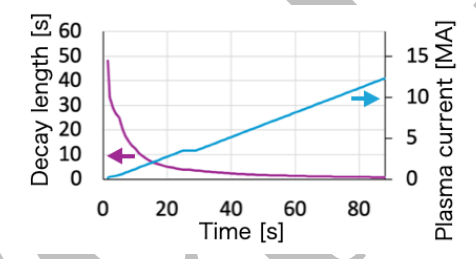


FIG. 2 Time evolution of decay length and plasma current during ramp-up phase

The FW data with optimized limiter shape has been prepared [8]. The limiter is separated to inboard limiter and outboard limiter, and each of them are installed near the toroidal center of a sector. The width and height of the limiter are 300 mm and 30 mm, respectively. The surface of the limiter is designed to be optimal curve to evenly distribute the surface heat load for limiter configuration plasma. The FW data consists of 3600 (toroidal) \times 1365 (poloidal) meshes, corresponding to the maximum mesh size of 30 mm in the toroidal direction and 20 mm in the poloidal direction.

2.2 FEM analysis for plasma facing unit

The applicability of the PFU design was evaluated through a time-transient coupled thermal-structural analysis. Two heat flux scenarios were simulated based on the expected FW heat load. One scenario corresponds to the location where the plasma touches the limiter at final moment of the limiter configuration during ramp-up phase, characterized by an instantaneous high heat flux. the other scenario involves a square-wave heat flux representing the highest heat flux deposited on the limiter during the flat-top phase. Both heat flux scenarios were applied iteratively to investigate the behaviour of plastic deformation. The mock-up model of the PFU, known as tungsten monoblock structure, is illustrated in Fig.3. Four tungsten blocks are perforated and skewered by an F82H steel pipe, with an interlayer material joint the two components. Heat flux is uniformly applied to the upper surface of the tungsten blocks, while coolant flows inside the F82H pipe to remove the heat. Based on previous study, copper and titanium were selected as interlayer material in this study. Copper is widely used in ITER divertor designs with copper alloy pipes due to its high plastic deformability and ability to buffer thermal stress. However, in this design, copper raises concern due to the large mismatch in the coefficient of thermal expansion (CTE) between

copper and F82H, which may induce significant thermal stress. Titanium is proposed as an alternative interlayer material, aiming to suppress thermal stress due to its intermediate CTE between tungsten and F82H, as supported by preliminary study [19]. The cooling water condition was assumed to be 290 degrees Celsius, 15.5 MPa pressure, and a flow velocity of 5 m/s. A swirl-tape-inserted pipe or an equivalent heat sink was assumed, with a swirl tube twist tape thickness of 2 mm and a twist ratio of 2. A heat transfer coefficient of 120 kW/m²·°C was applied to the inner surface of the pipe based on reference [20]. The mechanical properties of the materials without neutron irradiation were referred from previous studies[21-24]. The von-Mises stress and its composition were analyzed and discussed to evaluate the structural applicability of the PFU design.

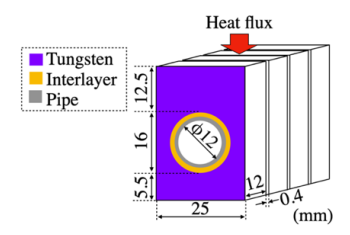


FIG. 3 Design of tungsten monoblock

3. RESULT AND DISCUSSION

3.1 Heat load on limiter

The time evolution of the heat flux distribution on the limiter is presented in Fig. 4. The horizontal axis represents the toroidal mesh number, while the vertical axis corresponds to the poloidal angle θ_{pol} , as defined in Fig. 1(c). The Inboard limiter spans poloidal angles from 94° to 231°, whereas the outboard limiter covers the ranges of 0° to 94° and 273° to 360°. At 1.5 seconds, plasma ignition occurs on the inboard side. Following ignition, the heat flux distribution gradually expands in accordance with the growth of the plasma shape during the ramp-up phase. At 27 seconds, the maximum heat flux reaches 2.8 MW/m² at the toroidal center of limiter. One second later, the plasma transitions from limiter configuration to divertor configuration, result in sharp decrease in heat flux as plasma detaches from the limiter. Power deposition shirts primarily to the divertor area. At 88 seconds, the plasma enters the flat-top phase, during which no significant heat flux is observed on the limiter. As the plasma heating increases, power deposition of the far SOL begins to appear on the limiter around 120 second. The heat flux distribution pattern changes, with higher heat fluxes observed at the toroidal edges of the limiter. The change is attributed to the composition of the heat flux. During the limiter configuration plasma, the plasma touch point is closest to the core plasma, resulting in a large qu and small incident angle. In contrast, during the divertor configuration plasma, the core plasma is farther from the FW, leading to a reduced q//, but the incident angle at limiter toroidal edges becomes large. In the flat-top phase, the heat flux evolves slowly, with the peak heat flux reaching 1.9 MW/m² at 800 seconds. The flat-top phase continues for approximately two hours, and plasma rampdown begins at 7330 seconds. At 7460 seconds, the plasma returns to the limiter configuration, but almost no power is deposited on the limiter from 7350 seconds.

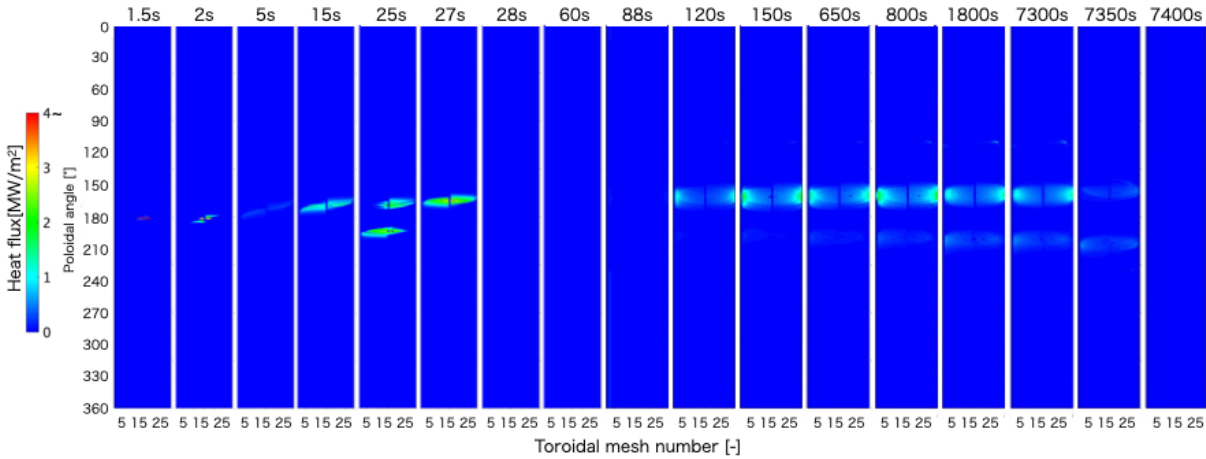


FIG. 4 Time evolution of charged particle heat load distribution on limiter

The locations exhibiting peak heat fluxes during ramp-up and flat-top phase are the focus of this analysis. To investigate the behaviour of the heat flux at adjacent surfaces, the time evolution of heat fluxes at peak locations as well as at their adjacent toroidal center and edge positions, is presented in Fig. 5(a) and 5(b). As shown in Fig. 5(a), an instantaneous high heat flux is observed during the ramp-up phase, localized exclusively at toroidal center of the limiter. In contrast, Fig. 5(b) reveals that during the flat-top phase, elevated heat fluxes are present at both toroidal edges of the limiter.

Based on the time evolution of charged particle heat load, the heat load scenario applied on the tungsten monoblock was defined, as illustrated in Fig. 5(c). For the ramp-up phase scenario, a consistent heat flux increase pattern was applied, with the peak heat flux reaching 2.8 MW/m². In the flat-top phase scenario, a total heat flux of 2.4 MW/m² was applied, which includes both charged particle heat load and other contributing components such as radiation heat load, charge exchange and ripple loss. In the simulation, the heat flux was applied for 20 seconds to allow the model to reach thermal equilibrium, followed by a 20-seconds cooling period with no heat flux. Each cycle spans 40 seconds, and a total of three cycles were simulated.

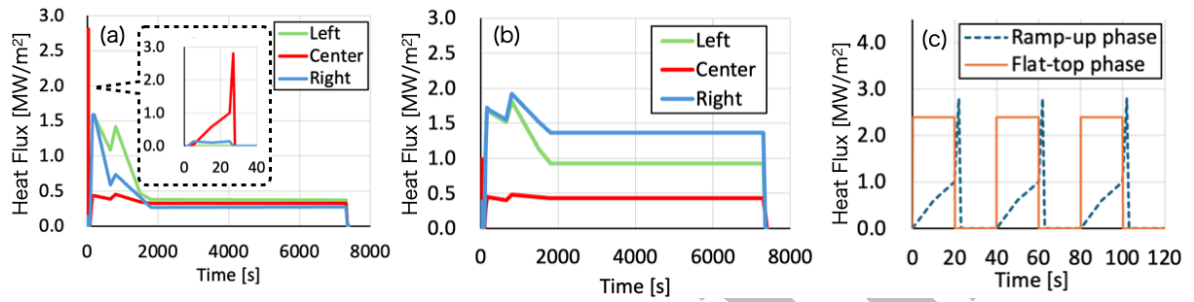


FIG. 5 Heat fluxes on limiter: Time evolution of charged particle heat load on (a) the location of peak heat flux during ramp-up phase, and (b) during flat-top phase. (c)Simulated heat load applied to the tungsten monoblock

3.2 Thermal stress of plasma facing unit

The time evolutions of the maximum temperature of each material with in the PFU simulation are shown in Fig. 6. In the cases with ramp-up phase heat load (Fig. 6(a) and 6(b)), a characteristic high-temperature spike is observed, caused by the instantaneous high heat flux. A notable difference in temperature behavior is seen in F82H, where only a slight temperature increment occurs with titanium interlayer. In the cases with the flat-top phase heat load (Fig. 6(c) and 6(d)), the temperature of each material gradually approaches thermal equilibrium under a continuous 20-seconds heat flux. The maximum temperature of tungsten is higher with titanium interlayer due to its low thermal conductance. Conversely, F82H exhibits a lower temperature, which is advantageous for protecting the F82H pipe, as it serves acritical role as the pressure boundary in the cooling system.

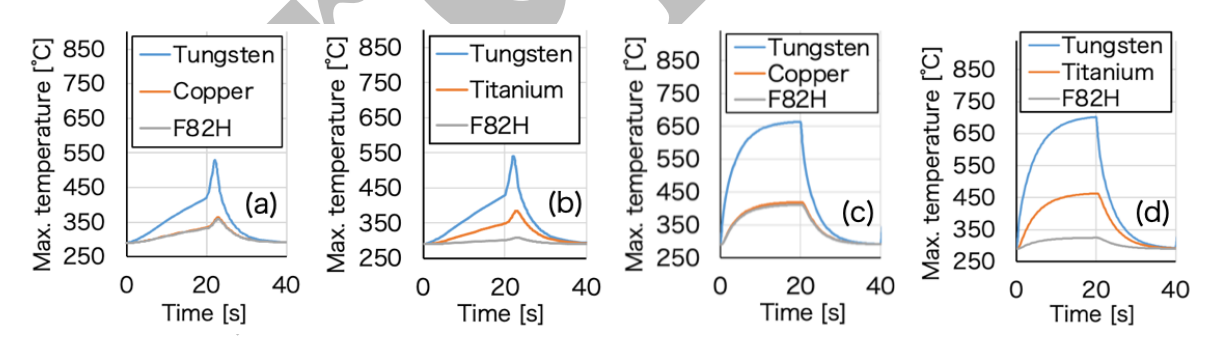


FIG. 6 Time evolution of the maximum temperature for each material with (a) copper interlayer at ramp-up phase, (b) titanium interlayer at ramp-up phase, (c) copper interlayer at flat-top phase and (d) titanium interlayer at flat-top phase

To investigate the reason for the temperature variation, the temperature distribution at the time of maximum temperature for a single monoblock section was extracted and is shown in Fig. 7. In the case with a titanium interlayer (Fig. 7(b) and 7(d)), the temperatures of the F82H pipe, which protrudes three-dimensionally from the side of the monoblock, are lower than in Fig. 7(a) and 7(c). This is attributed to lower thermal conductivity of titanium compared to copper. Specifically, the thermal conductivity of the titanium is approximately 5% that of copper, and even lower than that of F82H. While the copper interlayer efficiently conducts heat from the top surface, the titanium interlayer impedes heat transfer, causing the heat to bypass it and follow the shortest available path. As a result, the heat distribution becomes more circumferentially uniform outside the interlayer.

The flat-top phase scenario exhibits greater temperature variation, and it is well known that the thermal stress is generated by temperature gradients. Therefore, the thermal stress under the flat-top phase scenario is further investigated, focusing on the 20-second mark when the material reaches its maximum temperature.

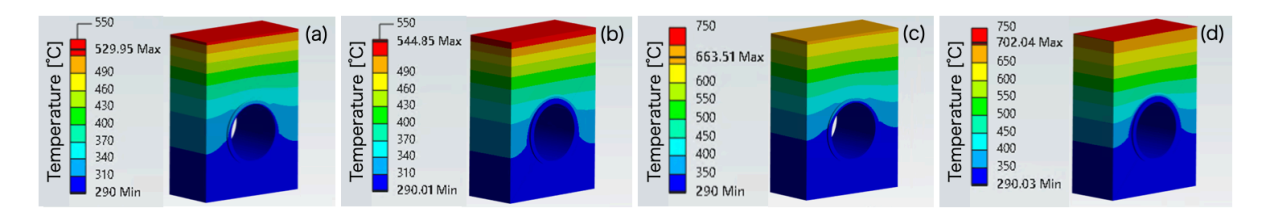


FIG. 7 Temperature distribution of the tungsten monoblock at the time of maximum temperature: (a) copper interlayer during ramp-up phase, (b) titanium interlayer during ramp-up phase, (c) copper interlayer during flat-top phase, and (d) titanium interlayer during flat-top phase

The von Mises stress distribution of the tungsten monoblock at the time of maximum temperature is shown in Fig. 8(a) and 8(b). A significant reduction in stress can be observed when comparing Fig. 8(b), which applied titanium interlayer, to Fig.8(a), which applied copper interlayer. In case of the copper interlayer (Fig. 8(a)), the stress is lower due to the plastic deformation. Fig. 8(c) presents the plastic strain distribution of the copper interlayer after three heat load cycles. The entire copper interlay has undergone plastic deformed as a result of the combined effect of thermal expansion and mechanical stress.

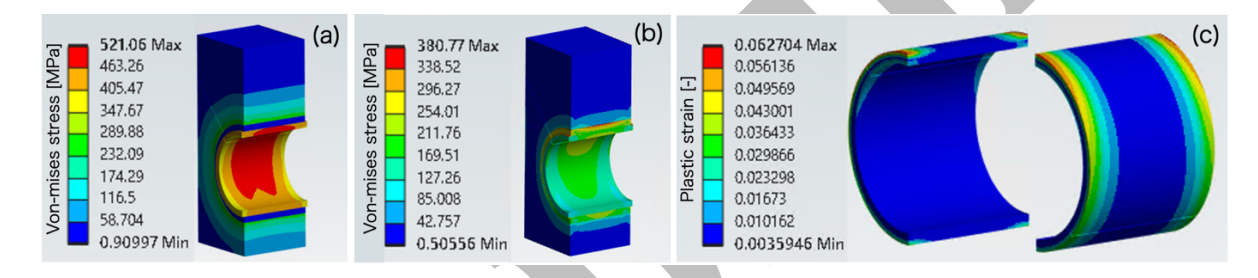


FIG. 8 Structure analysis of tungsten monoblock: Von-mises stress at time of 20 seconds with (a) copper interlayer model and (b) titanium interlayer model. (c) Plastic deformation of copper interlayer after three heat load cycles.

Focusing the F82H pipe, the von-mises stress distributions at the time of maximum temperature for each interlayer material are shown in Fig. 9, revealing significant differences. With the copper interlayer, the stress on the inner surface of the pipe reaches 488 MPa, particularly concentrated beneath the monoblock. In contrast, with the titanium interlayer, the highest stress appears on outer surface of the pipe, located between adjacent monoblocks. The stress on the inner surface of the pipe with titanium interlayer is 233 MPa, which representing a 52% reduction compared to the copper interlayer case.

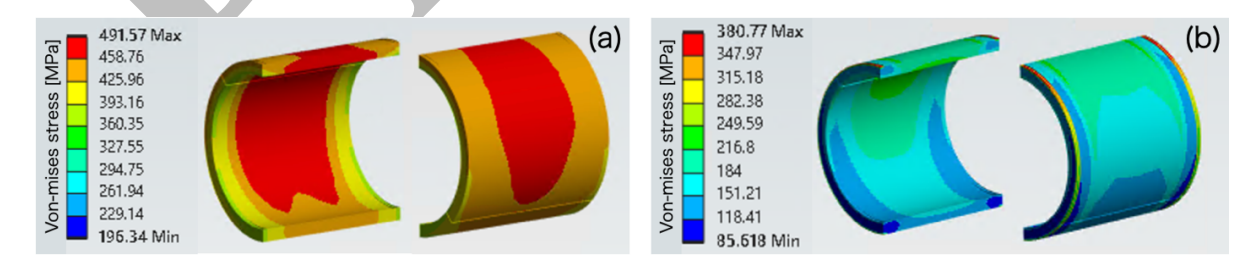


FIG. 9 Von-mises stress of F82H pipe at time of 20 seconds with (a) copper interlayer and (b) titanium interlayer

The simulated plastic strain of the F82H pipe is shown in Fig. 10. The plastic deformation of the pipe and the progressive propagation of the strain with an increasing number of heat load cycles can be clearly observed. This behavior is critical, as the F82H pipe serves as pressure boundary component.

To investigate the stress components, the maximum principal stress distributions of F82H pipe for each interlayer material are shown in Fig. 11. Positive values indicate tensile stress, while negative values represent compressive stress. According to the result, the inner surface of the pipe is subjected to tensile stress. When combined with

high von Mises stress, plastic deformation, and inner pressure, the inner surface with the copper interlayer experiences extremely critical condition that may lead to crack initiation. However, the application of a titanium interlayer significantly reduces the von-misses stress and helps maintain the stress within the elastic deformation range, making it more suitable for use as a pressure boundary component.

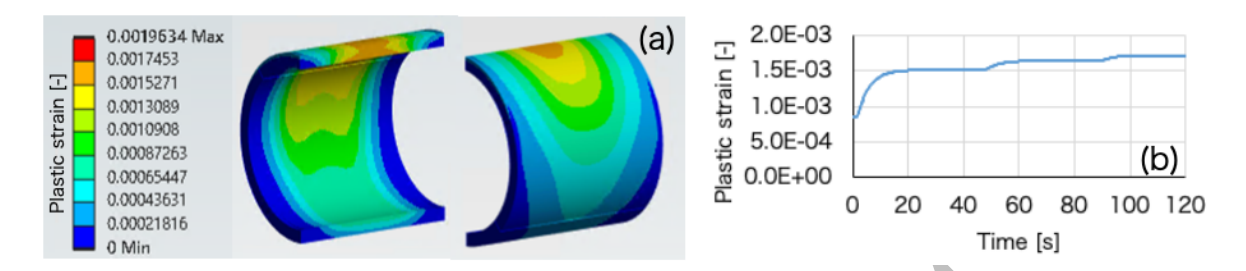


FIG. 10 Plastic strain of F82H pipe with copper interlayer: (a) plastic strain distribution after three cycles (b) time evolution of maximum plastic strain

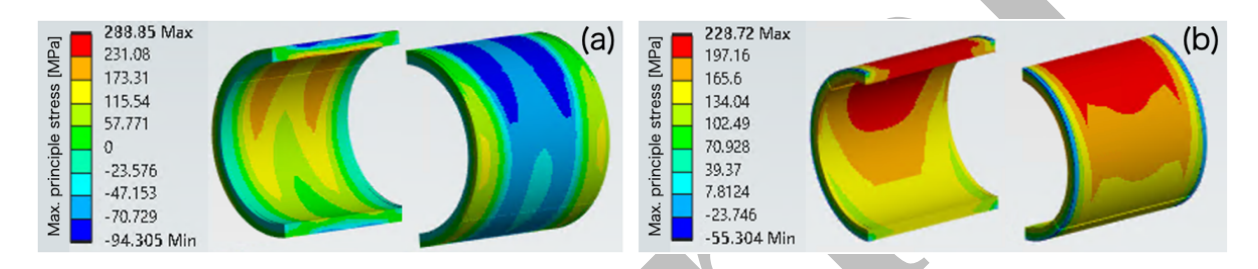


FIG.11 Maximum principal stress of F82H pipe at the time of 20 seconds with (a) copper interlayer and (b) titanium interlayer

Conclusion

In this study, the heat load on the limiter during pulsed plasma operation scenario in JA DEMO was evaluated, and the suitability of the plasma-facing unit was investigated. The charged particle heat load was evaluated at selected time points throughout the plasma operation. Plasma ramp-up begins with touching on the inboard limiter. During the ramp-up phase, the peak heat flux reaches 2.8 MW/m² at 27 seconds after initiation. Due to the transient from limiter configuration to divertor configuration of plasma, the time evolution of the heat flux exhibits a spikelike pattern. Once the plasma enters the flat-top phase and heating continues, the heat flux evolves more gradually. The peak heat flux during this phase reaches 1.9 MW/m² at 800 seconds after initiation. The flat-top phase is sustained for approximately two hours, after which the plasma ramp-down begins. During this phase, the plasma is guided to touch the outboard limiter for a controlled termination. Based on heat load scenario on the limiter, this study investigated the thermal and mechanical behavior of tungsten monoblock structures with different interlayer materials, copper and titanium, under ramp-up and flat-top phase heat load conditions. The simulation results revealed that the choice of interlayer material significantly influences the temperature distribution, stress concentration, and plastic deformation within the structure. The copper interlayer, while effective in conducting heat, led to higher von Mises stress and plastic deformation due to high thermal expansion, particularly on the inner surface of the F82H pipe. This condition poses a risk for crack initiation due to the combined effects of tensile stress, thermal expansion, and internal pressure. In contrast, the titanium interlayer demonstrated superior performance in mitigating stress by 52%, maintaining elastic deformation for the F82H pipe. The titanium interlayer also shifted the stress concentration to the outer surface of the pipe, thereby enhancing the structural integrity of the pressure boundary component. Overall, the titanium interlayer offers a promising solution for improving the durability and reliability of monoblock structures in high-heat-flux environments, making it a suitable candidate for fusion reactor applications.

ACKNOWLEDGEMENTS

This work was carried out within the framework of the Broader Approach DEMO Design Activity. The simulation work was carried out using the JFRS-1 supercomputer system at Computational Simulation Centre of International Fusion Energy Research Centre (IFERC-CSC) in Rokkasho Fusion Institute of QST (Aomori, Japan).

REFERENCES

- [1] BARRETT, T.R., et al., Design and technologies for plasma-facing wall protection in EU DEMO, Nucl. Fusion **59** (2019), 056019
- [2] VIZVARY, Z., et al., European DEMO first wall shaping and limiters design and analysis status, Fusion Eng. Des. 158 (2020) 111676
- [3] MAVIGLIA, F., et al., Impact of plasma-wall interaction and exhaust on the EU-DEMO design, Nucl. Mater. Energy **26** (2021) 100897
- [4] YOU, J.H., et al., Limiter for DEMO wall protection: initial design concepts & technology options, Fusion Eng. Des. 174 (2022) 112988
- [5] RICHIUSA, M.L., et al., The integrated engineering design concept of the upper limiter within the EU-DEMO LIMITER system, Fusion Eng. Des. **202** (2024) 114329
- [6] TOBITA, K., et al., Japan's efforts to develop the concept of JA DEMO during the past decade, Fusion Sci. Technol., **75** 2019, 372-383
- [7] CHEN, W., et al., Development of Poloidal horseshoe limiter concept for JA DEMO, IEEE Trans. Plasma Sci. **50**, 11, November 2022, 4233
- [8] CHEN, W., et al., Conceptual design of poloidal horseshoe limiter layout for JA DEMO, Fusion Eng. Des. 199 (2024) 114131
- [9] MIYOSHI, Y., et al., Analysis of peak heat load on the blanket module for JA DEMO, Fusion Eng. Des. **151** (2020) 111394
- [10] SUGIYAMA, S., et al., Development of pulsed plasma operation scenario and required conditions in JA DEMO, Nucl. Fusion **64** (2024) 076014
- [11] HAYASHI, N., Advanced tokamak research with integrated modeling in JT-60 Upgrade, Phys. Plasmas 17 5 (2010) 056112.
- [12] SHINYA, K., Equilibrium analysis of tokamak plasma, J. Plasma Fusion Res., 76 (2000) 479
- [13] EICH, T., et al., Scaling of the tokamak near the scrape-off layer H-mode power width and implications for ITER, Nucl. Fusion **53** (2013) 093031
- [14] KOCAN, M., et al., Impact of a narrow limiter SOL heat flux channel on the ITER first wall panel shaping, Nucl. Fusion 55 (2015) 033019
- [15] ASAKURA, N., et al., Development and application of SONIC divertor simulation code to power exhaust design of Japanese DEMO divertor, Process, **10** (2022) 872
- [16] EICH, T., et al., Inter-ELM power decay length for JET and ASDEX Upgrade: measurement and comparison with heuristic drift-based model, Phys. Rev. Lett. **107** (2011) 215001
- [17] GOLDSTON, R.J., Heuristic drift-based model of the power scrape-off width in low-gas-puff H-mode tokamaks, Nucl. Fusion 52 (2012) 013009
- [18] LOARTE, A., et al., Power and particle fluxes at the plasma edge of ITER: Specifications and physics basis, in *Proc.* 22nd IAEA Fusion Energy Conference (2008) IT/P6-13
- [19] ZHONG, Z., et al., Microstructure and mechanical properties of diffusion bonded joints between tungsten and F82H steel using a titanium interlayer, J. Alloys Compd., **489** (2010) 545-551
- [20] MARSHALL, T. D., et al., Modeling the nukiyama curve for water-cooled fusion divertor channels, Fusion Technol., **39** 2P2 (2001) 849-855,
- [21] NOZAWA, T., et al., The status of the Japanese material properties handbook and the challenge to facilitate structural design criteria for DEMO in-vessel components, Nucl. Fusion **61** 11 (2021)116054
- [22] ITER Structural Design Criteria for in-Vessel Components (SDC-IC) Code, document G 74 MA 8 01-05-28 W 0.2, 2012.
- [23] FISHER, E.S., TENKEN, C.J., Single-crystal elastic moduli and the hcp→bcc transformation in Ti, Zr, and Hf, Phys. Rev. 135 (1964) A482
- [24] GORECKI, T., The relations between the shear modulus, the bulk modulus and Young's modulus for polycrystalline metallic elements, Mater. Sci. Eng., **43** (1980) 225–230